Nuclear Charge Radii of Neutron-Deficient Lead Isotopes Beyond $N = 104$ Midshell Investigated by In-Source Laser Spectroscopy

H. De Witte,[1] A. N. Andreyev,[2,3] N. Barré,[4] M. Bender,[5,6] T. E. Cocolios,[1] S. Dean,[1] D. Fedorov,[7] V. N. Fedoseyev,[8] L. M. Fraile,[8] S. Franchoo,[4,8,9] V. Hellemans,[10] P. H. Heenen,[5] K. Heyde,[10] G. Huber,[9] M. Huyse,[1] H. Jeppessen,[8] U. Köster,[5,*] P. Kunz,[9] S. R. Lesher,[1,†] B. A. Marsh,[8,11] I. Mukha,[1,‡] B. Roussière,[4] J. Sauvage,[4] M. Seliverstov,[7,9] I. Stefanescu,[1] E. Tengborn,[12] K. Van de Vel,[1,§] J. Van de Walle,[1] P. Van Duppen,[1] and Yu. Volkov[7]

[1]*Instituut voor Kern- en Stralingsfysica, K.U. Leuven, B-3001 Leuven Belgium*
[2]*Oliver Lodge Laboratory, University of Liverpool, Liverpool, L69 7ZE, United Kingdom*
[3]*TRIUMF, Vancouver BC, V6T 2A3, Canada*
[4]*Institut de Physique Nucléaire, F-91406 Orsay Cedex, France*
[5]*Service de Physique Nucléaire Théorique, Université Libre de Bruxelles, B-1050 Bruxelles, Belgium*
[6]*DAPNIA/SPhN, CEA Saclay, F-91191 Gif-sur-Yvette Cedex, France*
[7]*Petersburg Nuclear Physics Institute, 188350 Gatchina, Russia*
[8]*ISOLDE, CERN, CH-1211 Genève 23, Switzerland*
[9]*Institut für Physik, Johannes Gutenberg Universität, D-55099 Mainz, Germany*
[10]*Vakgroep Subatomaire en Stralingsfysica, University of Gent, B-9000 Gent, Belgium*
[11]*Department of Physics, University of Manchester, Manchester, M60 1QD, United Kingdom*
[12]*Chalmers University of Technology, SE-412 96 Göteborg, Sweden*

(Received 7 December 2006; published 16 March 2007)

The shape of exotic even-mass $^{182-190}$Pb isotopes was probed by measurement of optical isotope shifts providing mean square charge radii ($\delta\langle r^2\rangle$). The experiment was carried out at the ISOLDE (CERN) on-line mass separator, using in-source laser spectroscopy. Small deviations from the spherical droplet model are observed, but when compared to model calculations, those are explained by high sensitivity of $\delta\langle r^2\rangle$ to beyond mean-field correlations and small admixtures of intruder configurations in the ground state. The data support the predominantly spherical shape of the ground state of the proton-magic $Z = 82$ lead isotopes near neutron midshell ($N = 104$).

DOI: 10.1103/PhysRevLett.98.112502 PACS numbers: 21.10.Ft, 23.60.+e, 27.70.+q, 42.62.Fi

The subtle interplay between individual and collective behavior of a finite number of strongly interacting fermions leads to aspects of mesoscopic systems that can only be studied in atomic nuclei [1]. For neutron-deficient nuclides around the closed proton shell at $Z = 82$, this interplay leads to the appearance of states with different shapes at low excitation energy. These so-called shape coexisting states can be interpreted as particle-hole excitations across the closed proton shell gap [2] whereby the interaction of the valence proton particles and holes with the neutrons drives the nucleus into deformation. The phenomenon of shape-coexistence is subject to intensive experimental and theoretical studies [3,4]. Alpha-decay experiments have revealed a triplet of low-lying 0^+ states in the ^{186}Pb nucleus, which is located at neutron midshell between $N = 82$ and 126 [1]. Excited bands built on top of the 0^+ states were observed in $^{182-190}$Pb [5–10], and recent lifetime measurements confirmed the deformed character of the bands [11]. For ^{186,188}Pb, it was concluded that the ground state and the 2_1^+ state have a very different structure, the 0^+ ground state of predominantly spherical and the 2_1^+ state of predominantly prolate character. Monopole transition strengths between the 0^+ states were used to estimate the mixing between the normal and intruder configuration [12] and revealed limited configuration mixing in the ^{190,192,194}Pb ground-state wave function [13,14]. But as the excited 0^+ states become lower in energy when approaching $N = 104$ (^{186}Pb), the mixing could increase substantially.

Several theoretical models have been applied to describe the structure of the neutron-deficient lead isotopes with their coexisting and mixed spherical, prolate, and oblate states, such as phenomenological shape mixing calculations [13,14], symmetry guided shell model and interacting boson model truncations [15,16], and beyond mean-field approaches [4,17,18]. All models that provide a consistent picture of the available data suggest that the ground state of lead isotopes is dominated by spherical configurations, even when the prolate and oblate rotational bands come down very low in energy around $N = 104$, and the barrier that separates the corresponding structures in the total energy surface is very small. But all models also suggest that the low-lying 0^+ states have mixed configurations with different shapes that might affect observables. Most experimental data, however, concern transitions to the ground state, which depend on the structure of the initial state.

Observables that give detailed information on the ground-state wave function are charge radii determined in atomic spectroscopy. Their measurements revealed, for example, a sudden and dramatic change in the mean square charge radii ($\delta\langle r^2\rangle$) between ^{187}Hg and ^{185}Hg ($Z = 80$) that was interpreted as a change in the ground-state defor-

mation from weakly oblate to strongly prolate [19,20], and similar deviations from sphericity have been observed in the neutron-deficient platinum ($Z = 78$) isotopes [21]. No such transition has been seen for the lead isotopes down to ^{190}Pb ($N = 108$) [22].

In this Letter, we report on the first measurement of the isotope shifts in the atomic spectra of the very neutron-deficient even-even $^{182-188}$Pb isotopes and deduce the mean square charge radii which probes the lead ground state directly. By combining the in-source laser spectroscopy technique with efficient alpha detection, mean square charge radii data were extended well beyond the neutron midshell at $N = 104$, from ^{190}Pb to the short-lived ^{182}Pb ($T_{1/2} = 55$ ms), which was detected with a rate of about 1 ion per second. The isotope shift and hyperfine splitting obtained for the odd-mass lead isotopes and isomers will be the subject of a separate publication.

The radioactive lead isotopes were produced at the PSB-ISOLDE facility at CERN, in a proton-induced ($E_p = 1.4$ GeV) spallation reaction on a thick (50 g/cm^2) UC_x target [23,24]. The reaction products diffuse out of the target toward the ion source cavity, heated to around 2050 °C. In this cavity, the lead isotopes are selectively ionized in a three-step laser ionization process. With copper-vapor pumped tunable dye lasers, atomic electrons are promoted out of the $6p^2\ (1/2, 1/2)_0$ ground state toward a $6p7s\ (1/2, 1/2)_1$ excited state ($\lambda = 283.305$ nm). In a second excitation step, the $6p8p\ (1/2, 3/2)_2$ level is reached by a second tunable dye laser ($\lambda = 600.186$ nm). The final ionizing step is supplied by the pump laser.

In order to determine the isotope shift of the optical line, the first excitation step laser is set to a narrow linewidth of 1.2 GHz, and its frequency is scanned over the resonance. The laser power in the first excitation step is reduced to avoid line broadening caused by saturation. This results in a reduced on-line ionization efficiency of about 1% [25]. Because of Doppler broadening in the hot cavity, the total linewidth was 4 GHz.

After ionization and extraction, the radioactive ions of interest are accelerated to 60 keV, mass separated and subsequently implanted in one of ten identical 20 μg/cm^2 carbon foils, mounted on a rotating wheel. A Si-detector (area 150 mm^2, thickness 300 μm), placed behind the foil, measures the α-radiation during a fixed implantation time. After this period, a new wavelength is set, and a fresh carbon foil is introduced by turning the wheel. The implanted lead ions are counted via their characteristic α-decay, and the intensity of the α lines as a function of the laser frequency reveals the optical isotope shift (see Fig. 1). The heavier isotope ^{190}Pb was measured via its β-decay in a similar way using a dedicated $\beta\gamma\gamma$ setup. The in-source laser spectroscopy technique was first used in Gatchina [26]. More details can be found in [27,28].

To determine the absolute wavelength calibration and the shape of the resonance curve, laser scans using the mass separated ion current of the stable isotope ^{208}Pb were performed regularly. In addition, the laser power in the first excitation step was recorded and used for normalizing the measured intensities over laser power fluctuations. For every mass, measurements with a fixed reference frequency, at regular time intervals (every third measurement point), were used to monitor the overall stability of the production, ionization, and detection system, except for ^{182}Pb (too low production rate).

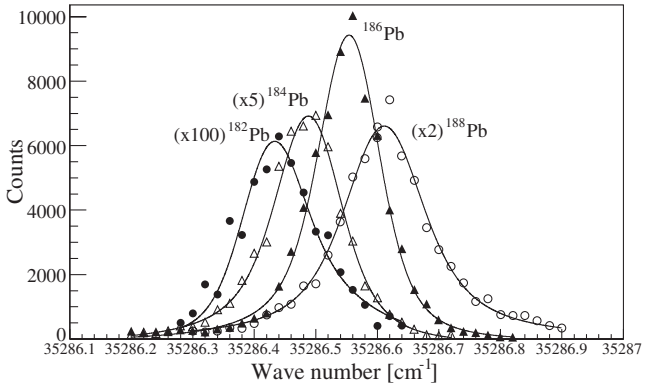

FIG. 1. Alpha intensity versus wave number for the even-even lead isotopes ^{188}Pb ($E_\alpha = 5980$ keV), ^{186}Pb ($E_\alpha = 6335$ keV), ^{184}Pb ($E_\alpha = 6626$ keV), and ^{182}Pb ($E_\alpha = 6921$ keV).

Figure 1 shows the obtained frequency scans. The curves are fitted with a convolution of a Gaussian and a Lorentzian, deformed to take into account the laser line asymmetry. From the centroid position, the isotope shift relative to ^{208}Pb, $\delta\nu^{A,208}$, is deduced. Details of the data analysis are presented in [29,30].

The isotopic change of the charge radius $\delta\langle r^2\rangle_{A,A'}$ was deduced from $\delta\nu_{A,A'}$ through the standard procedure as explained in [31]. The results are given in Table I. The isotope shift in the 723 nm atomic optical transition from $6p^2\ (^1D_2)$ to $6p7s\ (^3P_1)$ and the mean square charge radius of ^{190}Pb had been measured previously by collinear laser spectroscopy [22], yielding a value of $\delta\langle r^2\rangle = -0.840(10)$ fm^2 in agreement with our result (Table I) and proving the reliability of the present technique.

Figure 2 shows the mean square charge radii for the lead, mercury, and platinum isotopes. The data are compared to the droplet model predictions [32] assuming zero deformation ($\beta_2 = 0$). The deviation from the spherical droplet model predictions increases when going down from the $Z = 82$ closed proton shell. The large deviation observed for the ground state of the odd-mass mercury isotopes [19,20] and the odd- and even-mass platinum isotopes [21] around $N = 104$ has been interpreted as due to the onset of strong prolate deformation. In case of lead, a modest deviation is observed, and Fig. 3 shows the difference between experimental charge radii and the droplet model prediction. To highlight possible shape effects, isodeformation lines are shown for $\beta_2 = 0.1$ and 0.15. From ^{196}Pb downwards, the spherical droplet model predictions deviate from the data, with an underestimation around 0.1 fm^2 from ^{190}Pb to ^{184}Pb. Introducing a static deforma-

TABLE I. Isotope shifts $\delta\nu_{\mathrm{exp}}^{A,208}$ in atomic transitions and $\delta\langle r^2\rangle_{\mathrm{exp}}$ in mean square charge radii relative to ^{208}Pb, deduced from this work. The tabulated errors reflect only the isotope shift uncertainties; the total errors are 0.025 fm^2 for ^{182}Pb, 0.013 fm^2 for $^{183-185}$Pb, and 0.010 fm^2 for $^{186-190}$Pb, including errors on the electronic factor and mass shifts.

Isotope	$T_{1/2}$ [s]	I	$\delta\nu_{\mathrm{exp}}^{A,208}$ [GHz]	$\delta\langle r^2\rangle_{\mathrm{exp}}$ [fm^2]
^{190}Pb	71	0^+	−15.86(10)	−0.839(5)
^{189}Pb	51	$\frac{3}{2}^-$	−16.82(15)	−0.890(8)
^{189m}Pb	...	$\frac{13}{2}^+$	−17.35(20)	−0.918(8)
^{188}Pb	25.1	0^+	−17.57(12)	−0.930(6)
^{187}Pb	15.2	$\frac{3}{2}^-$	−18.78(12)	−0.993(6)
^{187m}Pb	18.3	$\frac{13}{2}^+$	−19.37(12)	−1.025(6)
^{186}Pb	4.82	0^+	−19.81(10)	−1.048(5)
^{185}Pb	6.3	$\frac{3}{2}^-$	−20.66(15)	−1.093(8)
^{185m}Pb	4.3	$\frac{13}{2}^+$	−21.26(15)	−1.125(8)
^{184}Pb	0.49	0^+	−21.74(10)	−1.150(5)
^{183}Pb	0.535	$\frac{3}{2}^-$	−22.95(15)	−1.215(8)
^{183m}Pb	0.415	$\frac{13}{2}^+$	−23.54(15)	−1.246(8)
^{182}Pb	0.055	0^+	−24.56(25)	−1.299(12)

tion in the droplet model with β_2 around 0.1 improves the agreement with the data for $^{184-190}$Pb, but is inconsistent with spectroscopic properties [3,11,32]. More realistic approaches that provide a good description of the coexisting bands in the neutron-deficient lead isotopes are the beyond mean-field calculations [4,18] and the Interacting Boson Model [16,33,34].

The model used in [4] mixes mean-field wave functions all having a different axial quadrupole deformation. Around midshell where the lead isotopes are soft, the collective wave function is spread over a large number of configurations, and the notion of spherical or deformed becomes ill defined. One can however still measure the importance of deformed configurations in the collective wave function by averaging the deformation of the mean-field wave functions with their weight in the former. A collective wave function with a distribution of components symmetric with respect to the spherical configuration will have a mean deformation close to zero and can be considered as spherical. This was indeed the case for the ground state of the lead isotopes studied in [4]. The resulting $\langle r^2\rangle$ values underestimate the experimental data and decrease too quickly with decreasing N (Fig. 3).

The global study of the ground-state properties within the same formalism presented in [18] points at the sensitivity of the isotope shifts to the details of the effective interaction. We have verified that the Skyrme interaction SLy4 used in [18] instead of SLy6 used in [4] brings only marginal changes. By contrast, the slight reduction of the pairing strength from [4] to [18] has a significant effect on the precise balance between excited prolate and oblate configurations but leads only to a very small increase in the mean deformation of the ground state. As seen in Fig. 3, this tiny modification leads to strongly different radii which overestimate the experimental data showing that isotope shifts are very sensitive to correlations in the lead ground-state wave functions.

The $\delta\langle r^2\rangle$ data are also compared to results from the configuration mixed IBM calculations where explicit mixing between the configurations resulting from regular $0p-0h$ and intruder $2p-2h$ and $4p-4h$ excitations across

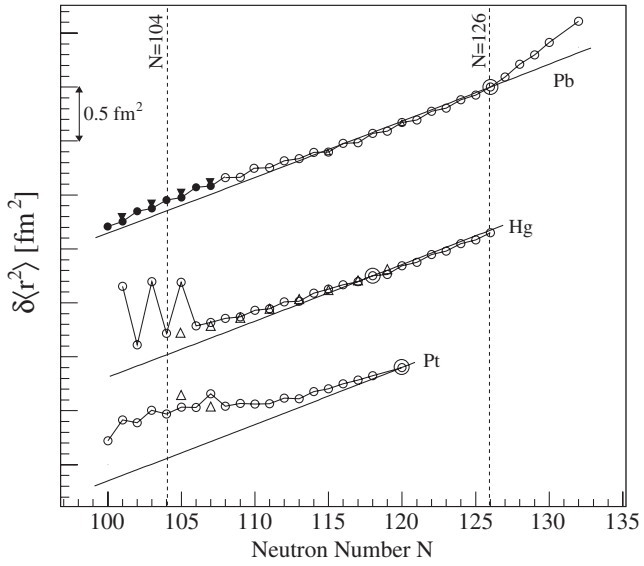

FIG. 2. Mean square charge radii for the lead [22,31,37], mercury [20], and platinum [21] isotopes, represented by the circles (ground state) and triangles (isomeric states), compared to the predictions of the droplet model [32], represented by the solid lines. The reference isotope for each element is circled. The error bars on the experimental results are smaller than the symbol size. The distance between the different chains is chosen arbitrarily for better display. The new data points from this work are displayed with full symbols.

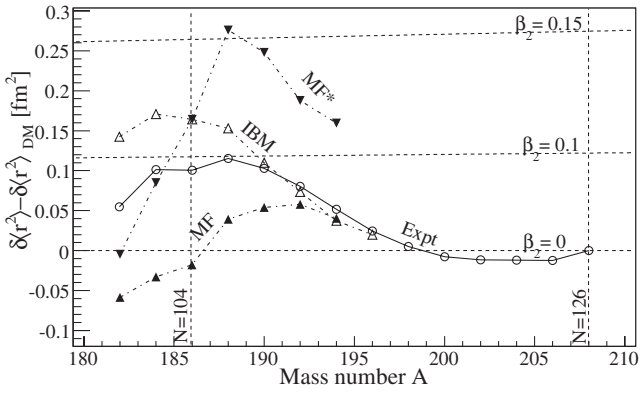

FIG. 3. Difference from the experimental mean square charge radii (Expt), the beyond mean-field calculations with normal [4] (MF) and decreased pairing [18] (MF*), and the IBM calculations (IBM) to the droplet model calculations for a spherical nucleus. Isodeformation lines from the droplet model at $\beta_2 = 0.1$ and 0.15 are shown.

the closed $Z = 82$ shell is considered [10,16,34]. A straightforward generalization of the operator representing the square radius [33] leads to the form

$$\langle r^2 \rangle = \langle r_c^2 \rangle + \langle \hat{P}_{\mathrm{reg}}^{-1}(\gamma_{\mathrm{reg}}\hat{N} + \beta_{\mathrm{reg}}\hat{n}_d)\hat{P}_{\mathrm{reg}} \rangle + \langle \hat{P}_{\mathrm{intr}}^{-1}(\gamma_{\mathrm{intr}}\hat{N} + \beta_{\mathrm{intr}}\hat{n}_d)\hat{P}_{\mathrm{intr}} \rangle,$$

whereby no distinction is made between $2p - 2h$ and $4p - 4h$ intruder excitations. The operator $\hat{N}$ takes into account the change of the radius with changing nucleon number while $\hat{n}_d$ accounts for deformation effects. The parameters $\gamma_{\mathrm{reg,intr}}$ and $\beta_{\mathrm{reg,intr}}$ describe the relative importance of the latter two effects within the different configurations considered, and $\hat{P}_{\mathrm{reg}}$ and $\hat{P}_{\mathrm{intr}}$ represent the projection operators onto the regular and intruder subspaces, respectively. We further focus on $\langle \hat{N} \rangle$ as the effect of $\langle \hat{n}_d \rangle$ on the radius is small in the lead isotopes.

Based on the intruder spin formalism [34] and on the similarity of the overall slope of the heavy lead, mercury, and platinum isotopes close to $N = 126$, the parameters γ_{reg} and γ_{intr} are taken equal (see Fig. 2). These parameters and their sign remain unchanged when crossing midshell. However, the decreasing number of bosons beyond midshell is corrected for in a similar way as in [34]. The magnitude of $|\gamma_{\mathrm{reg}}| = |\gamma_{\mathrm{intr}}| = 0.105\ \mathrm{fm}^2$ is obtained from the slope for $^{202-206}$Pb. Because the radius is decreasing when moving from ^{208}Pb to lighter isotopes, γ_{reg} takes on a negative sign. On the contrary, γ_{intr} should have a positive sign because the presence of intruder states introduces deformation into the ground state, hence increasing the nuclear radius relative to the global decrease. The results, using the ground-state wave functions as obtained in [10,35], are shown in Fig. 3. Important to note is that also in the IBM approach, small admixtures of intruder configurations in the lead ground state, as reported in [10,16,34], account for the observed deviation of $\delta\langle r^2 \rangle$ from the spherical droplet model evidencing the high sensitivity of $\delta\langle r^2 \rangle$ to tiny details of the ground-state wave function.

The optical isotope shifts and the mean square charge radii have been measured for very neutron-deficient lead isotopes beyond $N = 104$ midshell using the in-source laser spectroscopy technique. From ^{190}Pb downwards, the $\delta\langle r^2 \rangle$ data show a distinct deviation from the spherical droplet model suggesting ground-state deformation, but comparisons of the data with model calculations show that the $\delta\langle r^2 \rangle$ is very sensitive to correlations in the ground-state wave functions and that the lead isotopes stay essentially spherical in their ground state even at and beyond the $N = 104$ midshell region. This experiment has shown that the extreme sensitivity of the combined in-source laser spectroscopy and alpha detection allows us to explore the heavy mass regions very far from stability down to isotopes produced at a few ions per second (^{182}Pb). A newly developed ionization scheme for polonium atoms will allow us to extend this study to the very neutron-deficient polonium where the influence of shape coexisting states in the ground state is expected to be much larger and shape staggering has been reported [36].

We acknowledge the ISOLDE group, X. Grave, and J.-F. Clavelin (IPNO) for assistance and support by IUAP P5/07, FWO (Belgium), and EURONS No. Eu-FP6. Work by M. Bender was performed within the framework of L'Espace de Structure Nucléaire Théorique (ESNT).

*Present address: ILL, Grenoble, France
†Present address: University of Richmond, Richmond VA, USA
‡Present address: Universidad de Sevilla, Sevilla, Spain
§Present address: VITO, IMS, Mol, Belgium

[1] A. N. Andreyev *et al.*, Nature (London) **405**, 430 (2000).
[2] J. Wood *et al.*, Phys. Rep. **215**, 101 (1992).
[3] R. Julin *et al.*, J. Phys. G **27**, R109 (2001).
[4] M. Bender *et al.*, Phys. Rev. C **69**, 064303 (2004).
[5] J. Heese *et al.*, Phys. Lett. B **302**, 390 (1993).
[6] A. M. Baxter *et al.*, Phys. Rev. C **48**, R2140 (1993).
[7] G. D. Dracoulis *et al.*, Phys. Lett. B **432**, 37 (1998).
[8] J. F. C. Cocks *et al.*, Eur. Phys. J. A **3**, 17 (1998).
[9] D. G. Jenkins *et al.*, Phys. Rev. C **62**, 021302 (2000).
[10] J. Pakarinen *et al.* (to be published).
[11] T. Grahn *et al.*, Phys. Rev. Lett. **97**, 062501 (2006).
[12] K. Heyde and R. Meyer, Phys. Rev. C **37**, 2170 (1988).
[13] P. Dendooven *et al.*, Phys. Lett. B **226**, 27 (1989).
[14] G. D. Dracoulis *et al.*, Phys. Rev. C **67**, 051301 (2003).
[15] A. Frank *et al.*, Phys. Rev. C **69**, 034323 (2004).
[16] V. Hellemans *et al.*, Phys. Rev. C **71**, 034308 (2005).
[17] R. R. Rodriguez-Guzman *et al.*, Phys. Rev. C **69**, 054319 (2004).
[18] M. Bender *et al.*, Phys. Rev. C **73**, 034322 (2006).
[19] J. Bonn *et al.*, Phys. Lett. B **38**, 308 (1972).
[20] G. Ulm *et al.*, Z. Phys. A **325**, 247 (1986).
[21] F. Le Blanc *et al.*, Phys. Rev. C **60**, 054310 (1999).
[22] S. B. Dutta *et al.*, Z. Phys. A **341**, 39 (1991).
[23] E. Kugler *et al.*, Nucl. Instrum. Methods Phys. Res., Sect. B **70**, 41 (1992).
[24] U. Köster *et al.*, Nucl. Instrum. Methods Phys. Res., Sect. B **204**, 347 (2003).
[25] U. Köster *et al.*, Nucl. Phys. A **701**, 441 (2002).
[26] G. D. Alkhazov *et al.*, Nucl. Instrum. Methods Phys. Res., Sect. B **69**, 517 (1992).
[27] V. N. Fedosseev *et al.*, Nucl. Instrum. Methods Phys. Res., Sect. B **204**, 353 (2003).
[28] A. N. Andreyev *et al.*, Eur. Phys. J. A **14**, 63 (2002).
[29] H. De Witte, Ph.D. thesis, K. U. Leuven, Leuven, 2004.
[30] M. Seliverstov *et al.* (to be published).
[31] M. Anselment *et al.*, Nucl. Phys. A **451**, 471 (1986).
[32] W. D. Myers *et al.*, Nucl. Phys. A **410**, 61 (1983).
[33] F. Iachello and A. Arima, *The Interacting Boson Model* (Cambridge University Press, Cambridge, 1987).
[34] R. Fossion *et al.*, Phys. Rev. C **67**, 024306 (2003).
[35] V. Hellemans, Master's thesis, University of Gent, 2003.
[36] A. N. Andreyev *et al.*, Phys. Rev. Lett. **82**, 1819 (1999).
[37] U. Dinger *et al.*, Z. Phys. A **328**, 253 (1987).